Experimental investigations on nonlinear dynamics in supercontinuum generation with feedback

Nicoletta Brauckmann*, Michael Kues, Till Walbaum, Petra Groß, and Carsten Fallnich

Institute of Applied Physics, Westfälische Wilhelms-Universität, 48149 Münster, Germany

*brauckmann@uni-muenster.de

Abstract: A system for supercontinuum generation by using a photonic crystal fiber within a synchronously pumped ring cavity is presented. The feedback led to an interaction of the generated supercontinuum with the following femtosecond laser pulses and thus to the formation of a nonlinear oscillator. The nonlinear dynamical behavior of this system was investigated experimentally and compared with numerical simulations. Steady state, period doubling and higher order multiplication of the repetition rate as well as limit cycle and chaotic behavior were observed in the supercontinuum generating system.

OCIS codes: (320.6629) Supercontinuum generation; (320.7110) Ultrafast nonlinear optics; (320.7140) Ultrafast processes in fibers.

References and links

1. R. R. Alfano and S. L. Shapiro, "Emission in the region 4000 to 7000 Å via four-photon coupling in glass," Phys. Rev. Lett. **24**, 584–587 (1970).
2. R. R. Alfano and S. L. Shapiro, "Observation of self-phase modulation and small-scale filaments in crystals and glasses," Phys. Rev. Lett. **24**, 592–594 (1970).
3. J. K. Ranka, R. S. Windeler, and A. J. Stentz, "Visible continuum generation in air-silica microstructure optical fibers with anomalous dispersion at 800 nm," Opt. Lett. **25**, 25–27 (2000).
4. J. C. Knight, "Photonic crystal fibres," Nature **424**, 847–851 (2003).
5. P. St. J. Russell, "Photonic crystal fibers," Science **299**, 358–362 (2003).
6. J. M. Dudley, G. Genty, and S. Coen, "Supercontinuum generation in photonic crystal fiber," Rev. Mod. Phys. **78**, 1135–1184 (2006).
7. H. Zhang, S. Yu, J. Zhang, and W. Gu, "Effect of frequency chirp on supercontinuum generation in photonic crystal fibers with two zero-dispersion wavelengths," Opt. Express **15**, 1147–1152 (2007).
8. M. Lehtonen, G. Genty, H. Ludvigsen, and M. Kaivola, "Supercontinuum generation in a highly birefringent microstructured fiber," Appl. Phys. Lett. **82**, 2197–2199 (2003).
9. I. Hartl, X. D. Li, C. Chudoba, R. K. Ghanta, T. H. Ko, J. G. Fujimoto, J. K. Ranka, and R. S. Windeler, "Ultrahigh-resolution optical coherence tomography using continuum generation in an air-silica microstructure optical fiber," Opt. Lett. **26**, 608–610 (2001).
10. A. D. Aguirre, N. Nishizawa, J. G. Fujimoto, W. Seitz, M. Lederer, and D. Kopf, "Continuum generation in a novel photonic crystal fiber for ultrahigh resolution optical coherence tomography at 800 nm and 1300 nm," Opt. Express **14**, 1145–1160 (2006).
11. J. H. Frank, A. D. Elder, J. Swartling, A. R. Venkitaraman, A. D. Jeyasekharan, and C. F. Kaminski, "A white light confocal microscope for spectrally resolved multidimensional imaging," J. Microsc. **227**, 203–215 (2007).
12. D. J. Jones, S. A. Diddams, J. K. Ranka, A. Stentz, R. S. Windeler, J. L. Hall, and S. T. Cundiff, "Carrier-Envelope Phase Control of Femtosecond Mode-Locked Lasers and Direct Optical Frequency Synthesis," Science **288**, 635–639 (2000).
13. T. Udem, R. Holzwarth, and T. W. Hänsch, "Optical frequency metrology," Nature **416**, 233–237 (2002).

#119287 - $15.00 USD Received 29 Oct 2009; revised 14 Jan 2010; accepted 23 Jan 2010; published 24 Mar 2010

14. G. McConnell and E. Riis, "Ultra-short pulse compression using photonic crystal fibre," Appl. Phys. B **78**, 557–563 (2004).
15. F. Lu and W. H. Knox, "Generation of a broadband continuum with high spectral coherence in tapered single-mode optical fibers," Opt. Express **12**, 347–353 (2004).
16. J. M. Dudley and S. Coen, "Coherence properties of supercontinuum spectra generated in photonic crystal and tapered optical fibers," Opt. Lett. **27**, 1180–1182 (2002).
17. Z. Zhu and T. G. Brown, "Effect of frequency chirping on supercontinuum generation in photonic crystal fibers," Opt. Express **12**, 689–694 (2004).
18. G. Genty, J. M. Dudley, and B. J. Eggleton, "Modulation control and spectral shaping of optical fiber supercontinuum generation in the picosecond regime," Appl. Phys. B **94**, 187–194 (2009).
19. E. Räikkönen, G. Genty, O. Kimmelma, M. Kaivola, K. P. Hansen, and S. C. Buchter, "Supercontinuum generation by nanosecond dual-wavelength pumping in microstructured optical fibers," Opt. Express **14**, 7914–7923 (2006).
20. J. C. Travers, S. V. Popov, and J. R. Taylor, "Extended blue supercontinuum generation in cascaded holey fibers," Opt. Lett. **30**, 3132–3134 (2005).
21. P. S. Westbrook, J. W. Nicholson, and K. S. Feder, "Grating phase matching beyond a continuum edge," Opt. Lett. **32**, 2629–2631 (2007).
22. D.-I. Yeom, J. A. Bolger, G. D. Marshall, D. R. Austin, B. T. Kuhlmey, M. J. Withford, C. M. de Sterke, and B. J. Eggleton, "Tunable spectral enhancement of fiber supercontinuum," Opt. Lett. **32**, 1644–1646 (2007).
23. P. M. Moselund, M. H. Frosz, C. L. Thomsen, and O. Bang, "Back-seeding of higher order gain processes in picosecond supercontinuum generation," Opt. Express **16**, 11954–11968 (2008).
24. Y. Deng, Q. Lin, F. Lu, G. P. Agrawal, and W. H. Knox, "Broadly tunable femtosecond parametric oscillator using a photonic crystal fiber," Opt. Lett. **30**, 1234–1236 (2005).
25. G. Steinmeyer, A. Buchholz, M. Hänsel, M. Heuer, A. Schwache, and F. Mitschke, "Dynamical pulse shaping in a nonlinear resonator," Phys. Rev. A **52**, 830–838 (1995).
26. M. Kues, N. Brauckmann, T. Walbaum, P. Groß, and C. Fallnich, "Nonlinear dynamics of femtosecond supercontinuum generation with feedback," Opt. Express **17**, 15827–15841 (2009).
27. NKT Photonics, "NL-PM-750 data sheet," http://www.nktphotonics.com/files/files/datasheet_nl-pm-750.pdf.
28. G. P. Agraval, *Nonlinear Fiber Optics*, (Academic Press, San Diego, California, 2007).
29. S. H. Strogatz, *Nonlinear Dynamics and Chaos*, (Perseus Books, Reading, Massachusetts, 1994).
30. H. Degn, "Effect of Bromine Derivatives of Malonic Acid on the Oscillating Reaction of Malonic Acid, Cerium Ions and Bromate," Nature **213**, 589–590 (1967).

1. Introduction

Supercontinuum (SC) generation is a nonlinear optical phenomenon where narrow bandwidth light becomes spectrally broadband due to, e.g., self-phase modulation, four-wave mixing, soliton fission and Raman scattering.

Since the first documentation of SC generation in 1970 by Alfano and Shapiro [1, 2] the development of microstructured fibers (MSF) as novel, highly effective nonlinear media with flexibly designable dispersion properties has boosted ultrabroadband supercontinuum generation [3–5]. Great progress has been achieved in the understanding of the complex mechanisms of supercontinuum generation as well as of its crucial parameter dependence, such as for instance the input wavelength, power, and pulse duration [6], as well as, the chirp [7] and the polarization [8].

Via the input pulse and fiber parameters supercontinua can be formed such that they can be used for several applications, such as optical coherence tomography [9, 10], fluorescence microscopy [11], optical frequency metrology [12, 13], and ultrashort pulse generation [14]. Beside adapting these usual input parameters to taylor specific supercontinua [15–17], the coherence properties could for example be improved by modulating the input temporal pulse shape [18], and certain spectral regions of the SC could be enhanced by two-color pumping [19], fiber cascades [20], fiber Bragg gratings [21] or long-period gratings [22].

Furthermore, the influence of optical feedback on the spectral SC composition was investigated in picosecond systems, where SC generation relies on seeded four-wave mixing [23, 24], as well as in the case of weaker nonlinearities of a single-mode fiber, where the dynamics of period multiplication and chaos were observed [25]. Numerical analysis of SC generation

#119287 - $15.00 USD Received 29 Oct 2009; revised 14 Jan 2010; accepted 23 Jan 2010; published 24 Mar 2010

in a feedback system with femtosecond pump pulses considering the complex simultaneous interplay of four-wave mixing, self-phase modulation, Raman scattering and higher-order dispersion was conducted recently by our group [26]. In that work, it was shown that femtosecond SC generation within a feedback loop constitutes a nonlinear oscillator, and that in certain parameter ranges steady state, period multiplication, limit cycle and chaos can be observed. With the introduction of feedback, additional parameters beside the conventional pulse and fiber parameters are given to influence the SC generation. Furthermore, it is possible to create specific time series via the effect of feedback, which might promote novel applications.

The work we present in the following is an experimental investigation building upon our recent theoretical work [26]. We experimentally study a femtosecond SC system with feedback, which is comparable to the numerically investigated system. The radio frequency measurement and for chaotic system behavior the optical spectrum have been adopted and their suitability for the measurement and identification of the different kinds of system dynamics are discussed.

First the experimental feedback setup (Section 2) and the numerical model including a feedback loop (Section 3) are introduced and the respective measurement techniques are presented. Then, the four different observed regimes of system dynamics and their characteristic features are experimentally identified and compared with our numerical simulations (Section 4).

2. Experimental setup

A SC was generated by focusing femtosecond pulses of a mode-locked laser into a MSF. To realize an optical feedback system, the MSF was incorporated into a ring cavity consisting of silver-coated mirrors and adjustable in length by a variable delay stage, as is sketched schematically in Fig. 1.

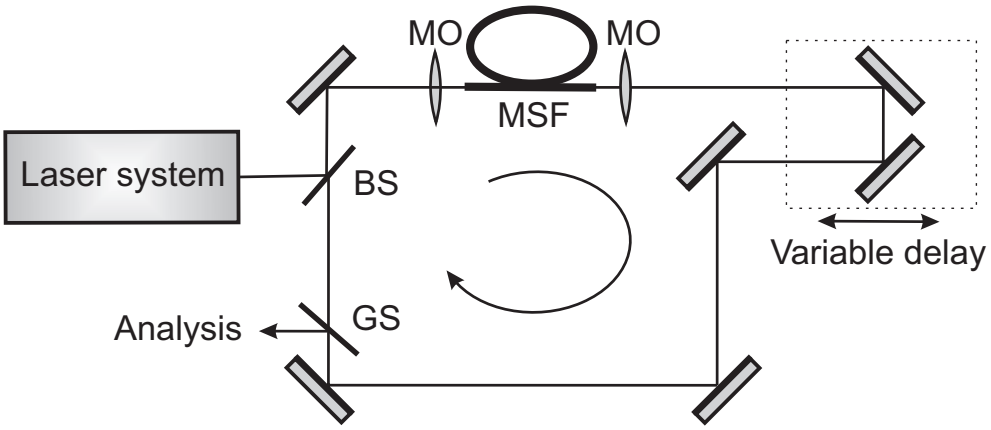

Fig. 1. Experimental setup: The laser system consisted of a Titanium:Sapphire laser, a Faraday isolator, and a prism pulse compressor; BS: pellicle beamsplitter, MSF: microstructured fiber, MO: 40x microscope objective, GS: uncoated glass substrate (For more details see text).

The laser system consisted of three modules: first a Titanium:Sapphire laser (Spectra Physics, Tsunami) and second a Faraday isolator to avoid reflections back into the laser resonator. After passing the third module, a compression stage consisting of two SF14 prims to compensate the dispersion of the Faraday isolator, a pulse duration (full width at half maximum) of 54 ± 6 fs was measured (APE autocorrelator model Mini and assuming a sech^2 intensity profile) at 775 nm central wavelength and 82 MHz repetition rate. For coupling these pulses into the ring cavity a pellicle beam splitter (BS) with a splitting ratio of 30:70 was used, so that only 30% pump

#119287 - $15.00 USD Received 29 Oct 2009; revised 14 Jan 2010; accepted 23 Jan 2010; published 24 Mar 2010

power is reflected to be coupled into the MSF. These high coupling losses were accepted in order to enhance the feedback efficiency. In the ring cavity the SC was generated by focusing the pump pulses with a 40x microscope objective (MO) into a 47 ± 2 mm long commercially available polarization maintaining MSF (NKT Photonics, NL-PM-750 [27]). The input power values in the measurements mentioned within the following sections refer to the effective power within the fiber, thus considering the coupling losses. The fiber was rotated such that the linearly polarized pump light was coupled into the fast axis, where the widest SC was generated and the polarization was maintained for all spectral components [8]. The fiber has two zero dispersion wavelengths (ZDW), one at 750 nm and the second at 1250 nm, such that there is an anomalous dispersion region only between these ZDWs. As the MSF was pumped in the anomalous dispersion region, soliton fission and soliton dynamics were the dominant effects leading to spectral broadening. The spectral broadening in dependence on the average input power was shown in [26], where also the interplay of the involved nonlinear effects was discussed. The generated SC was collimated behind the fiber with a second 40x MO. The cavity round trip was completed by the SC passing the pellicle beamsplitter, with a transmission efficiency of 70%, to be coupled back into the MSF. In order to arrange a superposition of the back-coupled SC with the next laser pulses, the cavity length was matched to the repetition rate of the driving laser system.

The reflection of an uncoated glass substrate (GS) was used to simultaneously measure the optical spectrum (optical spectrum analyzer, OSA: ANDO AQ 1425) and the radio frequency spectrum (silicon photo diode with rise time $\approx$1 ns, connected to a radio frequency spectrum analyzer: Advantest, TR 4131/E).

The total losses of the feedback ring cavity strongly depended on the quality of the facets of the MSF: The microstructured cladding showed capillary action, so that water of the air humidity entered into the fine air hole structure, resulting in changed dispersion and mode field properties at the entrance as well as at the exit of the fiber. As a consequence the coupling efficiency decreased with time from about 70 % to 50 %, but could be restored by cleaving. In addition to the temporal variation of the coupling efficiency, we observed a strong wavelength dependence of transmission and reflection properties of the optical components in the feedback path. To measure the feedback efficiency, the power at the output port with and without feedback was recorded, which yielded values between 20 % to 5 %.

3. Numerical implementation

The numerical implementation is described in detail in [26]; here we only repeat shortly, what is crucial for the understanding of the derived results presented in the following Section 4.

The numerical calculations are performed within two main steps: first the pulse propagation within the nonlinear fiber and second the interference of the generated SC with the new incoming laser pulse, thus providing the initial conditions for the next cavity round trip.

The pulse propagation within the nonlinear fiber was described by the generalized scalar nonlinear Schrödinger equation (GNLSE) and solved numerically using a split-step Fourier method, which is an established model to simulate light propagation in nonlinear waveguides [6, 26, 28].

For simulating the experimental feedback setup described in Section 2 the model of SC generation had to be extended by a feedback loop. Specifically after each numerical integration of the electric field along its propagation in the MSF a fraction of the SC was superimposed with the next incoming pump pulse, simply by adding up two data arrays one for each involved pulse. A delay τ for cavity detuning was implemented by an additional phase factor of the fed back SC pulse, consisting of a factor $i\omega\tau$ linear with the instantaneous light frequency ω and a constant factor $i\omega_0\tau$ with the carrier frequency ω_0. The linear factor is responsible for the temporal shift

#119287 - $15.00 USD Received 29 Oct 2009; revised 14 Jan 2010; accepted 23 Jan 2010; published 24 Mar 2010

τ in the time domain, while the constant factor sets the correct interference condition. With these modified initial conditions, the GNLSE was solved for the next propagation through the fiber.

In order to have comparable conditions to the experiments, a power fraction of 9% of the SC pulses was superimposed with the incoming pump pulses of the Titanium:Sapphire laser at each round trip. This cycle of adding up the fields of the two pulses and solving the GLNSE was repeated typically a few hundred times until the final system behavior was reached.

The fiber parameters (absorption coefficient α, nonlinear coefficient γ and dispersion coefficients β_k) were derived from the data sheet of the MSF (NKT Photonics, NL-PM-750 [27]) used in the experiments, as described in [26].

A fiber length of 45 mm and laser pulses with a hyperbolic secant field profile and a full width at half maximum pulse duration of 60 fs at a central frequency of 775 nm were chosen as input parameters. We note, that the numerical pulse parameters differ slightly from the experimentally determined ones, which is due to varying experimental conditions. Nevertheless, all numerically predicted system dynamics were also observed in our experiments.

To analyze the temporal evolution, which is specific for each regime of system dynamics, in the simulations both the temporal and spectral field components of the resulting SC were saved after each fiber propagation and before being superimposed with the next laser pulse. For the calculations an array size of 2^{16} data points was chosen for reliable results. This means, that two vectors, one including the temporal and one the spectral field components, each with 2^{16} complex values are created after each cavity round trip. The system state after each round trip is defined by either the temporal field component vector or by the spectral field component vector, which is one point in the $2 \cdot 2^{16}$ dimensional phase space ($A(\lambda_i)$, $\varphi(\lambda_i)$) with $i = 1...2^{16}$, spanned by the spectral amplitude $A(\lambda_i)$ and the spectral phase $\varphi(\lambda_i)$ of every simulated wavelength component. The classification of the system behavior in different regimes of system dynamics corresponds to different characteristic temporal evolutions of the system states. Since all 2^{16} field components are coupled due to the interplay of dispersion and nonlinear effects within the fiber, all components show the same system dynamics [25]. We checked this carefully for many examples and observed the same qualitative behavior for these components. For a consistent and clearly arranged classification of the system behavior in the following sections the evolution of only one wavelength component at 800 nm was plotted in a two dimensional cross section through phase space with its amplitude as radius and its phase as angle. The data generated during the transient phase (typically less than one hundred round trips) were not considered.

For a detailed frequency analysis of the temporal evolution and for comparison with the experimental data, the radio frequency spectrum $S_{\mathrm{rf}}(\nu_{\mathrm{rf}})$ was calculated. To retrieve the radio frequency spectrum, the optical spectrum $S(\lambda, n)$ after the nth cavity round trip was integrated over the whole spectral range to yield a single value, namely the pulse energy $W(n)$. Accordingly, the temporal evolution was discretized in steps of 12 ns, corresponding to the laser's repetition rate of 1/12 ns = 82 MHz. The radio frequency spectrum $S_{\mathrm{rf}}(\nu_{\mathrm{rf}})$ can then be derived from the discretized energy evolution by performing a Fourier transformation:

$$S_{\mathrm{rf}}(\nu_{\mathrm{rf}}) = FT\left(W(n)\right) = FT\left(\int S(\lambda, n)\, d\lambda\right). \tag{1}$$

To resolve detailed spectral features in the radio frequency spectrum, the Fourier transform was generated of at least 200 feedback round trips after the transient phase. Due to the discretization in the calculated radio frequency spectrum only modulation frequencies up to 41 MHz can be extracted. This frequency interval, however, includes all information about the modulation frequencies, as given by the Nyquist theorem. Higher frequencies that are experimentally detected are sidebands to the repetition rate and higher harmonics and do not contain new information. Because of this relation, measurements do have a mirror symmetry with respect to

#119287 - $15.00 USD Received 29 Oct 2009; revised 14 Jan 2010; accepted 23 Jan 2010; published 24 Mar 2010

41 MHz. However, to display characteristic features in comparison to the repetition rate, it is useful to show the whole radio frequency spectrum up to 82 MHz and thus the calculated radio frequency spectra are displayed up to 82 MHz throughout the paper, mirrored with a symmetry axis at 41 MHz.

For a well-arranged demonstration of the different system dynamics especially in phase space, the simulations were calculated without noise, so that the noise level in the radio frequency spectrum was reduced to the numerical noise floor (≈ -300 dB), which was much lower than the experimentally measured value (≈ -50 dB), and therefore is not observable in the following graphs.

4. Experimental and numerical results: Four different regimes of system dynamics

The different system dynamics identified from our numerical simulations can be classified into four regimes: steady state, period multiplication, limit cycle and chaos. Which kind of system dynamics is shown by the system, depends on a number of adjustable parameters, like for example the input pulse power and duration, the feedback efficiency, the dispersion introduced per feedback loop, and the temporal delay of the SC pulse with respect to the next pump pulse. All different regimes of system dynamics presented in this work could be obtained experimentally and numerically by adjusting the input pump power as well as the delay, while the other parameters were kept constant. The input pump powers used for the experiments and corresponding simulations were approximately matched, but we had no absolute measure for the cavity length at hand, and the dispersion additionally introduced in the experiment by optical elements in the feedback path (microscope objectives, etc.) was not taken into account for the simulations. The measurement and numerical implementation of the overall dispersion is subject of current investigations. Without the exact knowledge of all parameters, quantitative predictions of the system behavior seem unrealistic, but despite the discrepancy between experimental and numerical parameters each kind of system dynamics found in our numerics was also observed experimentally.

In the following the characteristics of each regime of system dynamics are presented. The phase space representation of each regime of the simulations is consulted as a demonstrative access to the system dynamics and for each regime the measured and simulated radio frequency spectra are compared.

4.1. Steady state

The elementary system dynamics observed in our system was the regime of steady state, where one system state was exactly reproduced after each cavity round trip.

Steady-state behavior was found numerically and experimentally, for example, at an input pump power of 5 mW. The phase space representation for a wavelength component at 800 nm from the simulated data are shown in Fig. 2(a). After each round trip, amplitude and phase assume the same value, which constitutes a fixed point in phase space, clearly indicating the SC feedback system being in steady state. In the according radio frequency spectrum [Fig. 2(b)], beside the dc peak at zero frequency, there is only one peak visible, namely the laser's repetition frequency at 82 MHz. The experimental results are displayed in Fig. 2(c), which shows the same two characteristic peaks at zero frequency and at the laser's repetition rate of 82 MHz like in the simulations.

The experimentally and numerically retrieved radio frequency spectra, both displaying only one characteristic frequency caused by the laser's repetition rate, are clearly indicating that the system was in steady state.

#119287 - $15.00 USD Received 29 Oct 2009; revised 14 Jan 2010; accepted 23 Jan 2010; published 24 Mar 2010

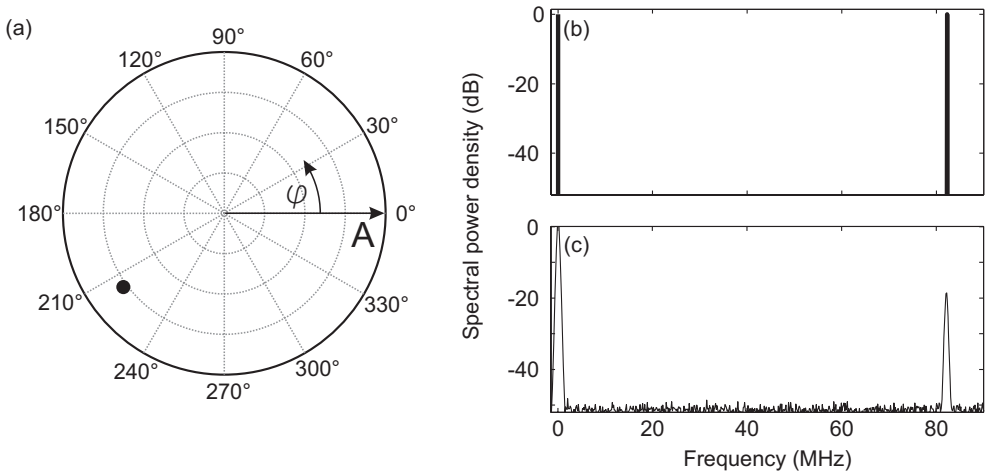

Fig. 2. Steady state: (a) simulated phase space representation for a wavelength component at 800 nm at an input power of 5 mW, (b) corresponding radio frequency spectrum, and (c) measured radio frequency spectrum.

4.2. Period multiplication

More complex was the regime of period multiplication, where a fixed point was not repeated after every round trip, but after a finite number of round trips. This behavior can be expressed in a fixed-point equation:

$$f^k(A) = A, \tag{2}$$

where A describes the system state (for example the complex electric field amplitude behind the MSF) and k is the order of period multiplication, i.e., the number of iterations, which is needed to reproduce the same system state. The function f describes one feedback round trip including both the superposition with the next pump pulse and the fiber propagation.

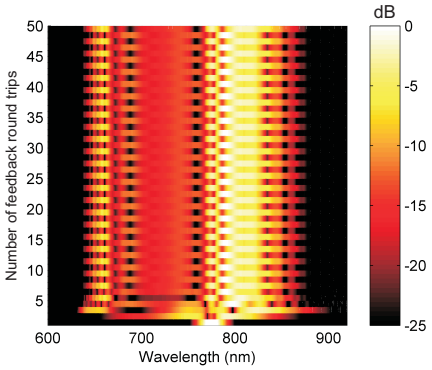

Fig. 3. Simulation of the SC evolution for a period-2 cycle at an average input power of 5 mW: optical spectrum in dependence of the number of feedback round trips.

The lowest order of period multiplication is two, where the system state is repeated after every second round trip, and which is called period-2 cycle. The fixed-point Eq. (2) for this case can be written as f(f(A))=A.

#119287 - $15.00 USD Received 29 Oct 2009; revised 14 Jan 2010; accepted 23 Jan 2010; published 24 Mar 2010

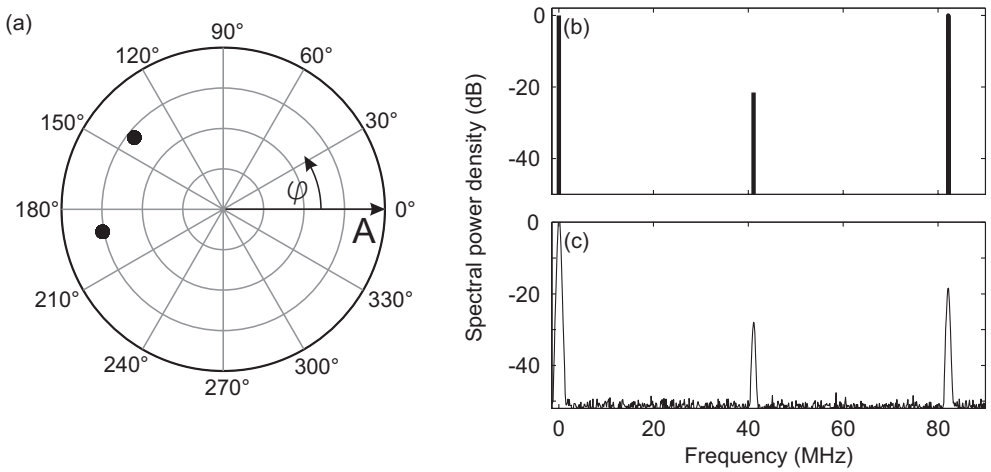

Fig. 4. Period-2 cycle: (a) simulated phase space representation for a wavelength component at 800 nm at an input power of 5 mW; (b) corresponding radio frequency spectrum and (c) measured radio frequency spectrum.

An example for this case is shown in Fig. 3 and Fig. 4. These traces were obtained at the same input power of 5 mW as in the case of steady state presented in Section 4.1, but the relative delay between SC and superimposed pump pulse has been changed in the experiment by 53 fs and in the simulation by 0.5 fs. In the spectral power density distribution shown in Fig. 3, each line corresponds to a spectrum, where the spectral power density is color-coded on a logarithmic scale. After a transient phase of less than 10 round trips, the system state alternated between two fixed spectra. This could also be observed in the time domain, where the system state alternated between two fixed pulse shapes.

The corresponding phase space representation at a wavelength component at 800 nm is shown in Fig. 4(a). For a period-2 cycle two fixed points in phase space were reached alternatingly. The difference of the system states of successive round trips are manifested in the amplitudes (Fig. 3) as well as in the phases [Fig. 4(a)] and can also be extracted from the pulse energy evolution. In the presented case the pulse energy after odd numbers of cavity round trips is 26% higher than that after even numbers. This originates from different interference conditions of each state with the next incoming pump pulse. As a result, the energy fluctuats with half of the laser's repetition rate, which can easily be detected in the experiment with a photodiode connected to a radio frequency analyzer.

As the two characteristic pulses were emitted alternatingly, each of these pulses was recreated only after two round trips, which means, effectively, a doubling of the period of the driving laser. As a result one would expect to detect a new characteristic frequency in the radio frequency spectrum, namely at half of the repetition rate of the driving laser, i.e., at 41 MHz.

The corresponding simulated and measured radio frequency spectra for a period two cycle at an average input power of 5 mW are shown in Fig. 4(b) and 4(c), where the expected additional frequency peak at 41 MHz appears in both graphs.

Scenarios of period multiplication of higher orders were also observed in the simulations as well as in the experiments. In Fig. 5 all orders of measured period multiplication from the order of three up to the order of eight are shown. Typically, the stability of period multiplication of higher orders is relatively low [29] and the parameter intervals for the existence of these solutions are small, which should make higher-order periods increasingly difficult to observe. Taking into account that one measured radio frequency spectrum is the result of about 10^6

#119287 - $15.00 USD Received 29 Oct 2009; revised 14 Jan 2010; accepted 23 Jan 2010; published 24 Mar 2010

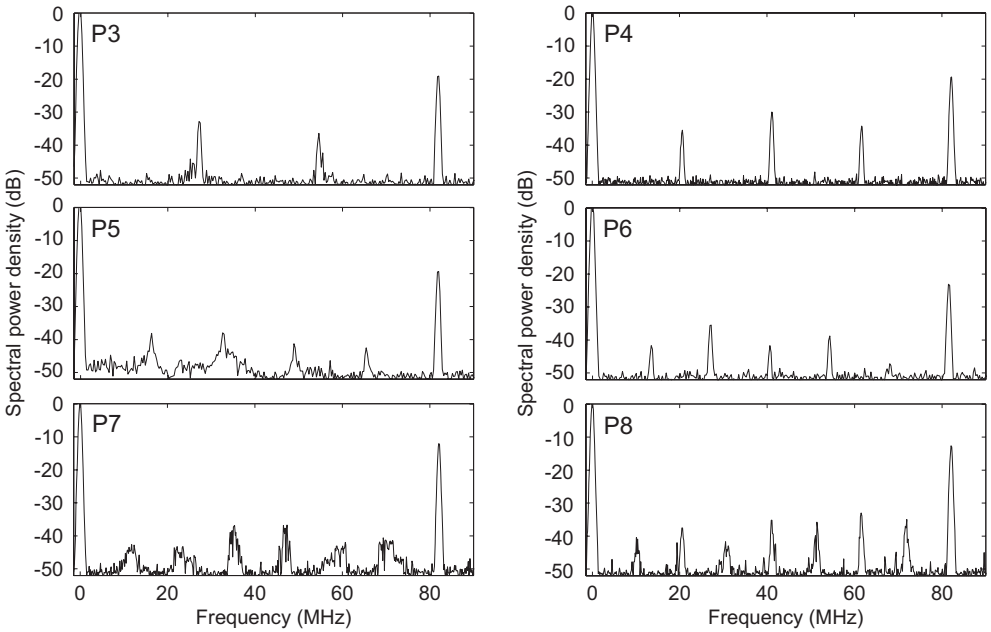

Fig. 5. Measured radio frequency spectra of period multiplication of order three (P3) up to the order of eight (P8).

pulses (assuming a measurement period of 0.1 s at a repetition rate of 82 MHz) and that the experimental system may drift out of and back into the regime during this time, it is obvious that a combination of different regimes might be measured. The slightly smeared frequency peaks of the period-5 and period-7 cycle in Fig. 5 could be an indication for such a behavior. In the experiment a period-8 cycle was indeed the highest order observed, while in our simulations period multiplication at least of the order of 16 (limited by the number of simulated round trips) was found.

In general, if a periodic attractor was reached, a certain system state was repeated after k cavity round trips according to the order of period multiplication k, leading to $k-1$ additional peaks in the radio frequency spectrum, equally spaced between the dc peak (around zero) and the peak of the laser's repetition rate at 82 MHz.

4.3. Limit Cycle

Beside period multiplication, also self-sustained oscillations were observed in our SC generation optical feedback system. This phenomenon is well known from several mechanical, chemical and biological nonlinear systems [29] such as for example spontaneous oscillations in chemical reactions like the Belousov-Zhaboutinsky reaction [30]. In phase space representation these self-sustained oscillations form a closed orbit, which is the reason why they are called limit cycles. Stable limit cycles are attractors very similar to stable fixed points. This means that during the transient phase the system asymptotically develops towards this attractor and finally remains there.

In our simulations several limit cycles were observed, for example at an input power of 6 mW. Its typical shape of a closed orbit is shown in the phase space representation for a wavelength component at 800 nm in Fig. 6(c). The red crosses indicate four system states, that are assumed after successive cavity round trips in the order they are numbered and as marked by the arrows.

#119287 - $15.00 USD Received 29 Oct 2009; revised 14 Jan 2010; accepted 23 Jan 2010; published 24 Mar 2010

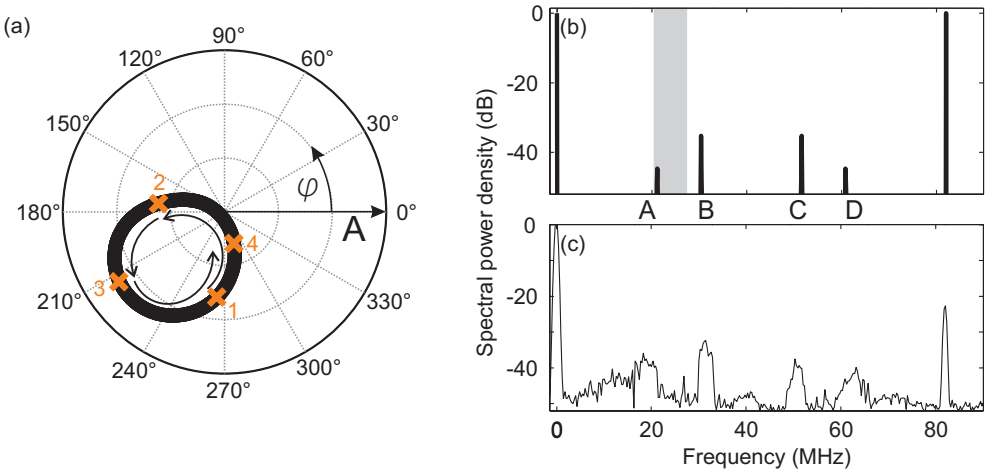

Fig. 6. Limit cycle: a) simulated phase space representation for a wavelength component at 800 nm at an input power of 6 mW; details are explained in the text. Radio frequency spectrum of b) simulated data for an input power of 6 mW (the gray-shaded area is explained in the text) and c) measured data for an input power of 7.5 mW.

The starting value on the limit cycle was randomly chosen. The arrows indicate, that a rotational frequency on the limit cycle can be defined, which describes the number of feedback round trips that are needed to complete one round trip on the limit cycle. In the presented example, more than three and less than four round trips are needed to pass the position of the first system state. Therefore, a rotational frequency is expected, which should appear in the radio frequency spectrum just above $82\,\mathrm{MHz}/4 = 20.5\,\mathrm{MHz}$ but lower than $82\,\mathrm{MHz}/3 = 27.3\,\mathrm{MHz}$, i.e. within the gray shaded area in Fig. 6(b). Indeed, the radio frequency spectrum derived from the numerical simulations reveals a frequency within this area, at 21.2 MHz [peak A in Fig. 6(b)]. The ratio of the rotational frequency and the laser's repetition rate is not rational; in the limit of a rational ratio, phase space would not show a full orbit, but discrete fixed points, which means that the system would be in the regime of period multiplication.

Furthermore, the different lengths of the arrows illustrate, that the velocity on the cycle is not constant, which means, that in Fig. 6(a) the system behavior is not described by a single frequency, but should contain at least a second frequency. This second frequency was found in the calculated radio frequency spectrum in Fig. 6(b) at 30.5 MHz (labeled as peak B).

In total, the calculated radio frequency spectrum shows four unequally spaced peaks: peak A at 21.2 MHz, representing the rotational frequency, peak B at 30.5 MHz, representing the velocity distribution, and peaks C and D, which are sidebands of the repetition rate corresponding to the peaks A and B and do not contain additional information. As no higher harmonics were observed, the energy fluctuations are a composition of two harmonic (sinusoidal) oscillations. Limit cycles with only one and even with three additional peaks in the radio frequency spectrum were observed as well, indicating a pure sinusoidal oscillation and a composition of three sinusoidal oscillations on the limit cycles, respectively.

With the insight gained by numerical simulations, limit cycles could also be identified experimentally: In Fig. 6(c) a measured radio frequency spectrum at an input power of 7.5 mW, slightly higher than in the simulations, is presented, which shows the same qualitative characteristic spectrum with four unequally spaced peaks (A, B, C, D) at similar frequencies as in the simulations. In general unequally spaced peaks in the radio frequency spectrum are clear indications of the system being in the regime of limit cycle.

#119287 - $15.00 USD Received 29 Oct 2009; revised 14 Jan 2010; accepted 23 Jan 2010; published 24 Mar 2010

4.4. *Chaos*

At relatively high input powers above 10 mW chaotic dynamics were dominant, which are missing any attractor like stable fixed points or stable limit cycles.

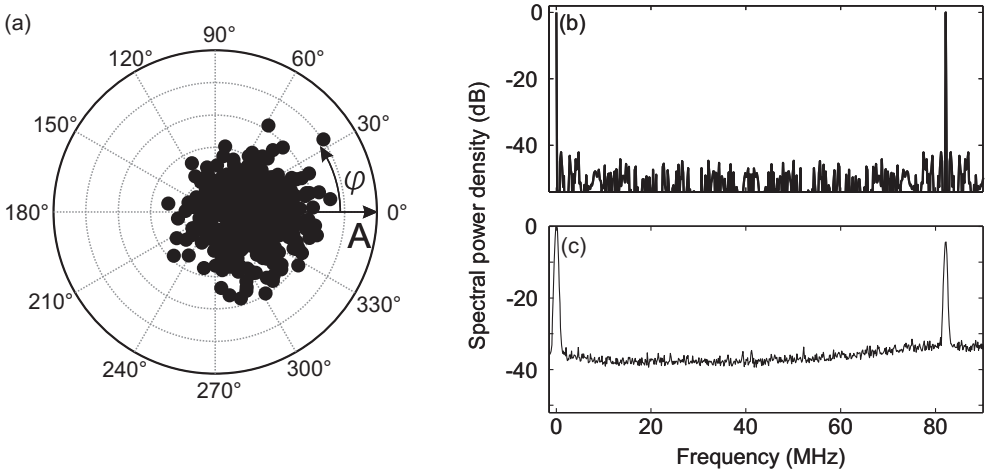

Fig. 7. Chaos: (a) simulated phase space representation for a wavelength component at 800 nm at an input power of 25 mW; (b) corresponding radio frequency spectrum and (c) measured radio frequency spectrum.

Figure 7 shows a cross section through phase space for a wavelength component at 800 nm as well as the according simulated and measured radio frequency spectra at an average input power of 25 mW in the chaotic regime are illustrated. In phase space the amplitude-phase coordinates of the 800 nm spectral component cover a wide area, with no recognizable regularity. Such distributions in phase space are typical for system dynamics without any attracting fixed points or attracting orbits [29], where no system state is ever exactly reproduced. The radio frequency spectrum gives again information about the involved frequencies. Except for the clear peak at the repetition rate of 82 MHz, no characteristic features could be identified in either of the two radio frequency spectra. Instead, the level of background was increased over the whole frequency range up to the repetition rate (in the measurements from the experimental noise level of -50 dB to -38 dB; in the simulations from the numerical noise floor below -300 dB to -50 dB). The absence of any prominent spectral feature demonstrated, that the system states showed no periodic order.

The random character of the phase space representation as well as the increased continuous background of the radio frequency spectra indicate strong fluctuations of system states. This chaotic behavior also has become manifested in the spectrum in Fig. 8(a), where 300 simulated spectra (gray lines) of successive cavity round trips are plotted. In contrast to the case of period multiplication (compare with Fig. 3(b)) no individual spectra can be identified. Instead, the 300 spectra overlap and combine to form the gray area.

To consider the integration time of the optical spectrum analyzer used in the experiments (around 1 ms per data point: each measured data point was an average of some 10^5 cavity round trips), the average spectrum out of the 300 spectra [solid gray lines in Fig. 8(a)] of successive round trips was calculated [solid black line in Fig. 8(a)] from the simulated data. In contrast to the spectrum without feedback (dotted red line) showing several detailed features, the fine structures are leveled out as an effect of averaging in the optical spectrum with feedback, resulting in a dramatically flattened spectrum. For comparison, two experimentally recorded spectra

#119287 - $15.00 USD Received 29 Oct 2009; revised 14 Jan 2010; accepted 23 Jan 2010; published 24 Mar 2010

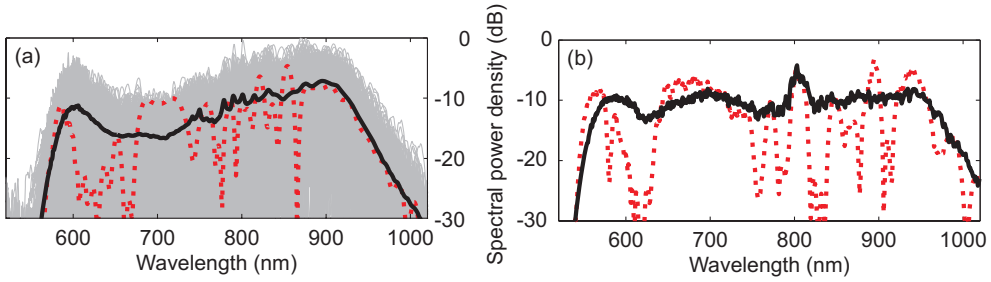

Fig. 8. Chaos: (a) examples of simulated optical spectra at an average input power of 25 mW from round trip number 200 to 500 (gray lines) and of the average optical spectrum without (dotted red line) and with feedback (solid black line), (b) example of the measured average optical spectrum at an average input power of 25 mW without (dotted red line) and with feedback (solid black line).

are plotted in Fig. 8(b), which were both measured at an input pump power of 25 mW, one with feedback (solid black line), and one with blocked feedback cavity (dotted red line). Here the same flattening effect as in the simulations is observed by introducing feedback: While the spectrum recorded without feedback displays distinct maxima and minima with spectral energy density varying by 31.0 dB, these features were reduced to 9.5 dB in the case of feedback.

While in the regime of period multiplication and limit cycle usually fine structures in the averaged optical spectra were maintained, flattened optical spectra are an indication for chaos, beside the characteristic radio frequency spectrum with an increased level of background.

5. Summary and conclusions

We investigated nonlinear dynamics in an experimental supercontinuum feedback system including a microstructured fiber in a ring cavity synchronously pumped with femtosecond laser pulses. Different kinds of nonlinear dynamics such as steady state, period multiplication up to the order of eight, limit cycle and chaos were experimentally found to be in good qualitative agreement with our numerical results. Since the spectral phase is not directly available in experiments, a direct representation especially of limit cycles were not possible. But it was identified, that the radio frequency spectrum delivers explicit characteristics to distinguish between all regimes of system dynamics. For steady state only the laser's repetition rate was visible, for period multiplication equally spaced and for limit cycle unequally spaced additional peaks appeared. For the chaotic regime not only the increased background level of the radio frequency spectrum was characteristic, but also the dramatically flattened optical spectrum.

The system behavior crucially depends on several parameters, such as the input power, pulse duration and chirp as well as the length, the efficiency and the dispersion of the feedback cavity. In the presented work only two of these parameters were varied, namely the input power and the delay. Only with those two free parameters, all presented regimes of system dynamics could be addressed in the simulations as well as in the experiment. Extended systematic parameter studies are the subject of our on-going investigations on SC generation with feedback.

With the nonlinear dynamics of, for example period multiplication it is possible to generate a repeating train of alternating pulse shapes. Such a light source might promote novel applications and as many applications would require flexible adjustability of the system dynamics and states, we will evaluate in the future how the SC spectra can be tailored by feedback control.

#119287 - $15.00 USD Received 29 Oct 2009; revised 14 Jan 2010; accepted 23 Jan 2010; published 24 Mar 2010

Acknowledgements

We gratefully acknowledge the support of D. Kracht and D. Wandt (both Laser Zentrum Hannover e.V., Germany) by providing us with a piece of microstructured fiber in order to enable a fast start of our experimental investigations. We also thank G. Steinmeyer (Max-Born-Institut Berlin, Germany) for helpful discussions.

#119287 - $15.00 USD Received 29 Oct 2009; revised 14 Jan 2010; accepted 23 Jan 2010; published 24 Mar 2010